Construction and Building Materials 30 (2012) 556–568

Contents lists available at SciVerse ScienceDirect

Construction and Building Materials

journal homepage: www.elsevier.com/locate/conbuildmat

An approach for estimating the capacity of RC beams strengthened in shear with FRP reinforcements using artificial neural networks

H.M. Tanarslan [a,*], M. Secer [a], A. Kumanlioglu [b]

[a] Department of Civil Engineering, Dokuz Eylul University, Buca, Izmir 35160, Turkey
[b] Department of Civil Engineering, Celal Bayar University, Muradiye, Manisa 45140, Turkey

ARTICLE INFO

Article history:
Received 31 May 2011
Received in revised form 14 November 2011
Accepted 2 December 2011
Available online 5 January 2012

Keywords:
RC beams
Shear strengthening
Neural networks
FRP

ABSTRACT

An artificial neural network model is developed to predict the shear capacity of reinforced concrete (RC) beams, retrofitted in shear by means of externally bonded wrapped and U-jacketed fiber-reinforced polymer (FRP) in this study. However, unlike the existing design codes the model considers the effect of strengthening configurations dissimilarity. In addition model also considers the effect of shear span-to-depth ratio (a/d) ratio at the ultimate state. It is also aimed to develop an efficient and practical artificial neural network (ANN) model. Therefore, mechanical properties of strengthening material and mechanical and dimensional properties of beams are selected as inputs. ANN model is trained, validated and tested using the literature of 84 RC beams. Then neural network results are compared with those 'theoretical' predictions calculated directly from International Federation for Structural Concrete (fib14), the American guideline (ACI 440.2R), the Australian guideline (CIDAR), the Italian National Research Council (CNR-DT 200) and Canadian guideline (CHBDC) for verification. Performed analysis showed that the neural network model is more accurate than the guideline equations with respect to the experimental results and can be applied satisfactorily within the range of parameters covered in this study.

1. Introduction

Reinforced concrete (RC) is a versatile, economical and successful construction material. It can be molded to a variety of shapes and finishes. In most cases it is durable and strong, performing well throughout its service life. However, poor design and construction, insufficient materials selection, and severe environmental effects like corrosion influence the performance of RC structures. Under these circumstances, these buildings may not withstand to earthquakes without severe damage and possible collapse because of the insufficient seismic performance due to one of or combination of the stated factors. In that manner, there is a significant need to perform sufficient assessment to these deteriorated RC structures and retrofit them for future seismic events. In this case, structural engineers have to make a selection of an appropriate earthquake retrofitting system by considering the cost-benefit assessment of the available alternatives in terms of both initial costs and life cycle cost manners. Developments in construction technologies and innovations in retrofit technologies add challenge in selecting technically, economically and socially acceptable solutions. A new retrofitting technique, external bonding fiber-reinforced polymer (FRP), contains almost all of these significant features. In addition, it has remarkable mechanical properties, such as durability, good corrosion resistance, non-magnetism, excellent fatigue behavior, and high strength to weight ratio.

Numerous tests have been conducted for appraising the effect of CFRP as a seismic retrofitting material [1–31]. At first, performance of FRP was demonstrated as a flexural strengthening material [1–3]. There is a common agreement that RC structures should be as ductile as possible so that enough warning of incipient collapse is given by large deflections and crack widths. According to the test results, the strengthening material could perform enough enhancements as flexural retrofitting material. Thereafter, researchers concentrated on investigating and/or examining the behavior of deficient structures strengthened in shear by FRP reinforcements [4–31].

Side bonding FRP application was primarily preferred for the initial shear enhancement studies due to its easy usage [4–9]. According to the test results, the contribution of side bonded FRP to the ultimate shear behavior is at a level that cannot be ignored. However, performed tests showed that achieving full capacity of FRP is almost impossible due to its major drawback, debonding [10,11]. In order to obstruct debonding, general opinion is to use anchorages. Two kinds of anchorages, mechanical and conventional anchorages, were suggested for obstructing debonding mechanism in the literature. However, it is clear that extra

* Corresponding author. Tel.: +90 232 4127047; fax: +90 232 4531192.
E-mail address: murat.tanarslan@deu.edu.tr (H.M. Tanarslan).

0950-0618/$ - see front matter © 2011 Elsevier Ltd. All rights reserved.
doi:10.1016/j.conbuildmat.2011.12.008

Nomenclature

a	length of shear span	p	shear strength reduction factor
A_s	area of steel in compression region	γ_r	additional reduction factor for FRP
A'_s	area of steel in tension region	k_v	bond reduction coefficient
Afs	area of CFRP shear reinforcement	k_1	modification factor regarding the concrete strength
b_w	width of beam cross section	k_2	modification factor regarding the FRP configuration
d_f	effective depth of the CFRP shear reinforcement	k_b	covering/scale coefficient
D_f	stress distribution factor	L_e	effective bond length of FRP reinforcement
E_f	elasticity modulus of FRP reinforcement	P_L	bond length coefficient
G_m	bonded joint specific fracture energy	P_w	strip width coefficient
f_{cd}	nominal concrete compressive strength of concrete	p_R	reduction factor due to local stress in corners
f_{cm}	average concrete tensile strength;	s_{uf}	FRP slip at debonding
f_{fed}	design value for the FRP effective stress	X	normalized maximum bond length
f_{fd}	design value for the ultimate FRP stress	β	orientation angle of the fibres
f_{fdd}	design value for the FRP debonding stress	ε_{fu}	ultimate tensile elongation of the fiber material in the FRP composite
$f_{fd\,max}$	maximum design stress in FRP	ε_{fe}	effective strain of FRP
f_{fu}	ultimate FRP tensile stress	y_{Rd}	partial factor for the resistance model
h	total height of the T section	y_f	partial factor for FRP reinforcement
h_{fe}	effective height of the bonded reinforcement	p_f	FRP reinforcement ratio
f_{cK}	concrete characteristic compressive strength		

productive power and labor cost is required for anchorage application [12,13]. On the other hand, U-jacketing and/or wrapping is an alternative method for obstructing debonding and utilizing the full performance of FRP [14–31]. Therefore, these strengthening techniques were tested to examine their success for obstructing debonding mechanism. Accordingly, both U-jacketing and wrapping methods performed well for obstructing debonding and proposed by researchers for utilizing the full capacity. In addition, test results indicated that the strengthening configuration; wrapping and U-jacketing have some behavior similarities in their ultimate strengthening effect [21,22].

The success of experimental studies produced growing demand for analytical investigations since predicting the ultimate shear strength of the strengthened RC structures is crucial. Therefore, several proposed analytical formulations have been developed to guide the design, detailing and installation of FRP based systems [38–42]. The developed analytical equations estimated the contribution of FRP reinforcements within certain limits but not accurately in some cases. In addition, researchers also produced some new methods for predicting the ultimate shear contribution [43]. The assumptions that were made while designating the behavior of the strengthened specimen did not resemble to actual behavior due to some special situations and that cause the calculated results to be different from the obtained shear capacity. There are several parameters that cause differences between the calculated and the obtained shear capacity. For example, some design guidelines neglect the difference between the two strengthening configurations and account them as the same though that methodology is definitely incorrect. In addition, codes also ignore the influence of the shear span-to-depth ratio (a/d) on ultimate shear behavior. These are the major assumptions that cause divergence towards the experimental results.

Since the ultimate shear behavior of strengthened RC beam is affected by many factors and parameters, artificial neural network (ANN) Method can be used as an effective tool to predict the ultimate shear behavior of strengthened RC beams [32–37]. Therefore, a neural network based model is developed in this study and performance of the ANN is outlined with respect to various design codes. The proposed ANN model considers the effect of a/d ratio which is not generally account in existing design codes. Furthermore, ANN model predicts the ultimate behavior of wrapped and U-jacketed specimens at the same time as ANN model contains data for both application schemes. 78 experimental data of strengthened RC beams were collected from literature. In addition, six shear deficient RC beams with different FRP configurations were tested in laboratory and added to the collected data's.

A parametric study is carried out to decide the inputs of the ANN model. As it is aimed to suggest a practical ANN model, the mechanical properties of strengthening material and mechanical and dimensional properties of beams are selected as inputs. The predicted ANN results are primarily compared with experimental FRP contributions of strengthened beams and then with the predicted results of theoretical guideline equations. International Federation for Structural Concrete (fib14) [38], the American guideline (ACI 440.2R) [39], the Australian guideline (CIDAR) [40], the Italian National Research Council (CNR-DT 200) [41] and Canadian guideline (CHBDC) [42] are the selected guidelines for evaluation. Performed analysis showed that the neural network model is more accurate than the guideline equations with respect to the experimental results and can be applied satisfactorily within the range of parameters covered in this study.

1.1. Experimental data

An extensive literature review has been carried out and seventy eight RC beams strengthened with wrapped and U-jacketed FRP reinforcements were collected from the literature [14–31]. Afterwards, six shear deficient RC beams were strengthened with different FRP configurations and tested in the laboratory by the authors. These test results are used to provide additional data for ANN.

The theoretically contribution of FRP to shear strength is obtained by subtracting the shear capacity of the beam V_{rc} (shear strength of concrete + shear strength of steel) from the ultimate shear strength. ACI 318 [44] detail estimation is one of the common methods for calculating V_{rc}. When the theoretically calculated shear capacity of the reference beam and the experimental shear capacity of the reference beam are compared, it is observed that the experimental shear capacity of the reference beam $V_{\exp}$, is most likely higher than the theoretically calculated value, V_{rc} [45]. It is hard to decide which V_{rc} to be used while obtaining V_f, the correlative contribution of FRP. In order to consider the difference and establish a more efficient ANN model, a combined scaling factor "m" was situated between calculated shear capacity of the control

beam V_{rc} and experiment shear capacity of the control beam V_{exp} (Eq. (1)).

$$m = \frac{V_{rc}}{V_{exp}} \tag{1}$$

The scaling factor is eliminating the divergences and making a correlation between reference and strengthened beams. This is also an alternative approach of separating the contributions from concrete, steel, and FRP based on the truss analogy led to little difference to the deduced FRP contribution. Thereafter "m" is used to find correlative contribution of FRP reinforcement to the shear capacity of the strengthened test beam (Eq. (2)). It must be noted that all strengthened test specimens had the same steel shear reinforcement arrangement as their respective reference beam.

$$V_f = V_{exp} - \frac{1}{m} \cdot V_{rc} \tag{2}$$

where V_f is the correlative contribution of FRP to shear strength of RC section, V_{exp} is the experimental shear capacity of the strengthened, m is the scaling factor and V_{rc} is the calculated shear capacity of the beam.

2. Experimental tests

An experimental program is conducted to provide experimental data for AN network. Six shear deficient (without shear reinforcement) RC beams are strengthened and tested in the experimental program. Test beams have different cross sections. Four of the test beams are T-beam and the remaining beams are rectangular sections. Rectangular beams are 200 mm wide, 350 mm high and 1700 mm long whereas the width of T-beam is 120 mm, depth is 360 mm and the flange width is 360 mm. The shear span to depth ratio (a/d) of all the test specimens is 5.0. All beams are designed with sufficient reinforcement and concrete strength to hinder flexural problems during the experimental program. Rectangular beams consist of four 20 mm diameter bars in the compression zone and four 20 mm diameter bars in the tension zone. T-section beams have three 20 mm diameter bars in the compression zone and three 20 mm diameter bars in the tension zone. The beams are strengthened with unidirectional CFRP wraps. The elastic modulus of wrap is 229 500 MPa. Its tensile strength and ultimate tensile strain is 4050 MPa and 1.7%, respectively. The adhesive that are used to bond the CFRP to concrete are composed of two parts. The direct tensile strength and secant tensile elastic modulus of epoxy are 3800 MPa and 30 MPa, respectively.

All specimens are tested up to failure. Sample failure modes of specimens are presented in Fig. 1. Fig. 1a is an example of U-jacketed T-beam that is failed due to debonding. In Fig. 1b rectangular crossed section beam that is totally wrapped with CFRP strips is tested. Accordingly, the specimen reached its flexure capacity under increasing loads. In order to perform load to the specimens, a loading column is designed with the hinges by the beam's free end. Loading column contained two hinges, a load cell and a hydraulic jack. Load is applied in cycles of loading and unloading. Load cycles are selected as they will help to evaluate the flexure and shear cracks propagations and their affect to behavior. Four linear variable differential transformers (LVDTs) are used to monitor displacements. In addition, eight strain gauges are attached at the section mid-height where shear cracks is expected to be developed. Shear capacity of each beam is presented in Table 1.

3. Artificial neural networks (ANNs)

An artificial neural network (ANN) is a simplified mathematical model or computational model that tries to simulate the structure and/or functional aspects of biological neural networks for engineering problems. It contains an interconnected group of artificial neurons and processes information using a connectionist approach to computation. In most cases, the ANN is an adaptive system that changes its structure based on external or internal information that flows through the network during the learning phase and can be used as a prediction tool for cases where the output solution is not available. Modern neural networks are non-linear statistical data modeling tools. They are usually used to model complex relationships between inputs and outputs or to find patterns in data [46–49].

ANN contains three main sections which are classified as, input layer, hidden (inner) layer, and the output layer. Input parameters are presented in the input layer and the solution of the problem are evaluated with the output layer. In between these layers, hidden layer is placed and provides help to the network in the learning process. These layers are created from neurons as shown in Fig. 2. The number of neurons of the input and output layers are determined in order to represent the characteristic of the existing problem accurately. Hidden layers can be formed with one or more layers and the number of neurons in the hidden layer is determined by the users. Connection weights (W_{ij}, W_{jk}) are used to connect all of the neurons in each layer to next layer neurons. In general, ANN model applications are performed in two steps. The network is created and trained at the first step and the network is validated with new input variables at the second step. During the training phase, net information is transmitted to output layer with connection weights by using Eq. (3).

$$net = \sum_{i=1}^{n} x_i W_{ik} \tag{3}$$

where net is the collection of information from each neuron with an artificial neural input value, x_i is input value and W_{ij} is connection weight value as presented in Eq. (3) and Fig. 3. Neuron output is calculated by transfer (activation) function. There are numerous transfer functions available for neural network models. These transfer functions can be in linear manner as step and rampage functions or non linear like Guassian, sigmoid, and hyperbolic tangent functions. The sigmoid transfer function is used to obtain neuron output (Eq. (4)).

$$f(\text{net}) = \frac{1}{1 + e^{-\text{net}}} \tag{4}$$

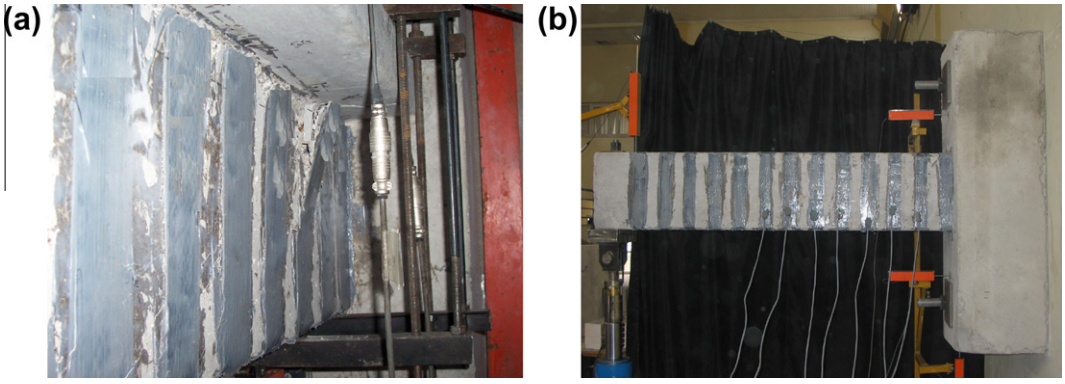

Fig. 1. Sample failure modes of specimen beams.

Table 1
Properties of test specimens.

Specimen specification (1)	f_{cd} (MPa) (2)	L (mm) (3)	a (mm) (4)	d (mm) (5)	a/d (6)	Wrapping scheme (7)	V_f (kN) (8)
TU90, 50 × 80	14.0	1700	1675	335	5.0	U-jacketed	40.48
TU90, 100 × 130	14.5	1700	1675	335	5.0	U-jacketed	29.68
TU90, 100 × 100	14.2	1700	1675	335	5.0	U-jacketed	49.78
TU90, 100,130	14.7	1700	1675	335	5.0	U-jacketed	17.58
RW90, 50 × 120	25.4	1700	1600	320	5.0	Wrapping	40.10
RW45, 100 × 350* [61]	24.7	1700	1600	320	5.0	Wrapping	45.60

1: T: T beam, R: Rectangular beam; #: orientation angle of the fibres; after comma CFRP configuration described (width × spacing), *Test data sets.

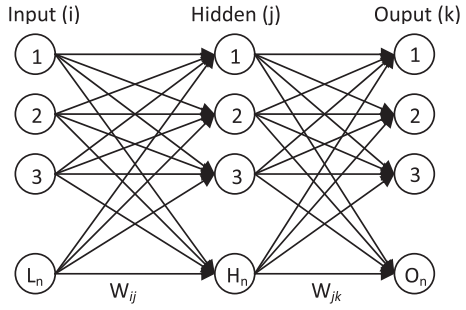

Fig. 2. An ANN structure.

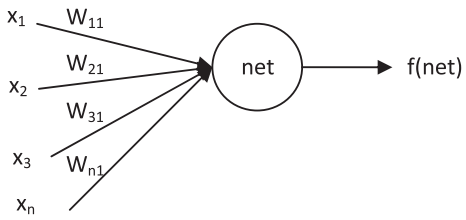

Fig. 3. Aneuron output.

where f(net) is a neuron output and the way how f(net) is obtained is plotted in Fig. 3. The ANN model's error is computed using neurons outputs and experimental values. If the error value is beyond the acceptable range, the network starts to backward pass from output layer to input layer [50–54]. Backward pass enables to redistribute error to the connection weights for determining their new values by using the training function. Consequently, backward pass all the connection weights between neurons are updated and iteration or epoch is accomplished by this manner. Finally, after the training step, the network uses the new input variables to predict the problem solution. Training algorithms are not given in details since these are quite common and can be found in any text on ANN. This paper rather focuses more on the application of feed-forward back-propagation algorithm to the experimental data using MATLAB [55].

4. Parametric study

A parametric study is carried out in order to decide which parameters to adopt in the neural network model. Therefore, three common guidelines, ACI 440.2R, CIDAR and fib14, are considered to designate the effects of parameters on ultimate shear behavior. It is clear that many important variables have an effect on FRP contribution. As a result, all the common parameters that influence the ultimate shear behavior of a strengthened beam; shear span-to-depth ratio, type of wrapping, effective height of the beam, elastic modulus of the FRP reinforcement, the angle between the principal fiber orientation and the longitudinal axis of the member; are considered.

4.1. Influence of type of wrapping scheme

Fig. 4 shows the effect of type of wrapping schemes over the guideline predictions. Type of wrapping scheme plays a key role for design guidelines while enhancing the FRP contribution. There is an almost a linear increase in FRP contribution for fib14 and ACI 440.2R when FRP spacing decreased, namely, application turned from FRP strip to FRP plate. However, the type of wrapping is more functioning for ACI 440.2R according to the slope of the curves. The increment tended to the decrease of spacing was provided a fast increment for CIDAR but it is not linear as other considered guidelines. It is clear that the highest contribution from the strengthening material is obtained when the shear span is covered with FRP and that is exactly the same for all guideline predictions.

4.2. Influence of the effective height of the beam

The variations of the predicted FRP contribution versus effective height of the beam for guidelines' are shown in Fig. 5. This is possibly the main parameter that affects the FRP contribution directly for the design guidelines. Predictions showed an almost linear increase in FRP contribution when effective height is increased. ACI 440.2R and fib14 showed similar sense to this parameter. Effective height is influencing CIDAR much more than ACI 440.2R and fib14 as can be seen from the slope that describes the CIDAR guideline.

4.3. Influence of the elastic modulus of the FRP reinforcement

FRP does not experience any yield and has a linear elastic behavior up to failure. Increase at elastic modulus of FRP influences its strain and stress behavior as well as its strength and stiffness. Therefore, elastic modulus of FRP plays a key role for increasing the strength of structure that was intended for strengthening.

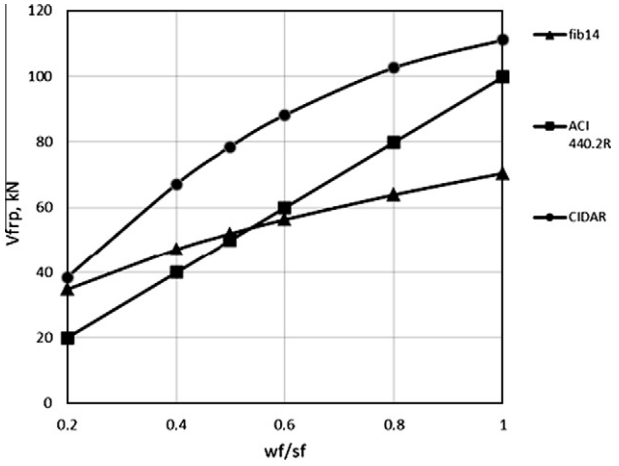

Fig. 4. Influence of type of wrapping scheme section.

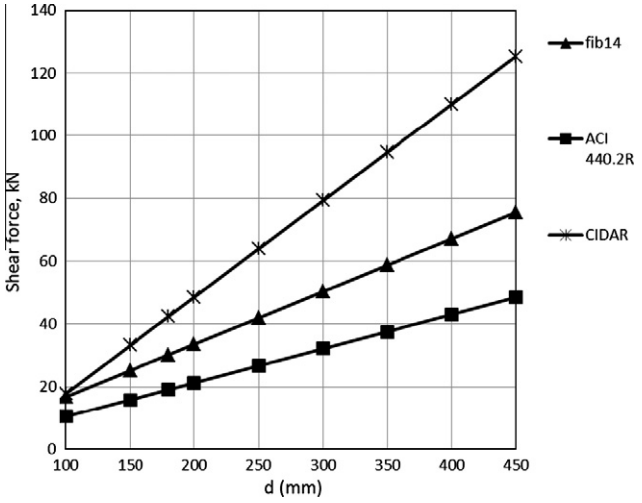

Fig. 5. Influence of the effective height of the beam section.

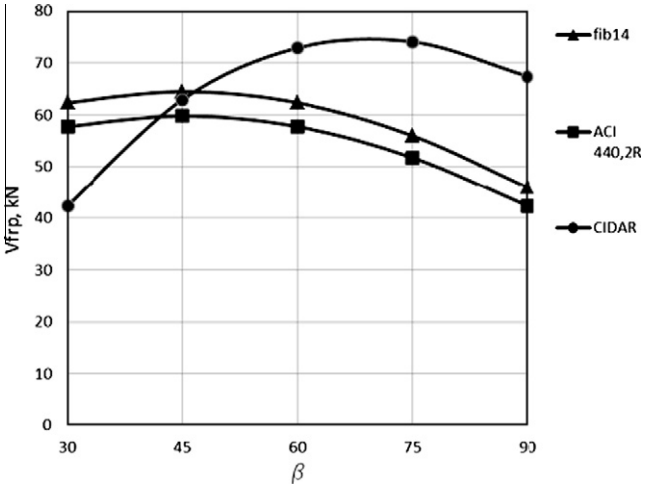

Fig. 7. Influence of the inclination of the FRP fibres.

Fig. 6 shows the influence of the FRP elastic modulus versus shear strength. As expected an increment tended to the increase of elastic modulus was obtained for the design guidelines. CIDAR and ACI 440.2R followed a similar tendency. However, fib14 design guideline uses some safety factors obliquely devoted to elastic modulus of FRP and this decreases its effect over the ultimate shear strength as can be seen from the slope of the curve that is agreed with fib14.

4.4. Influence of the inclination of the FRP fibres

Fig. 7 shows the influence of inclination of the FRP fibres. In this study, the influence of inclination of the FRP fibres, between 30° and 90°, is considered. As it is seen from Fig. 7, inclination angle has the same importance for design guidelines. ACI 440.2R and fib14 followed the similar tendency. For inclination angle 90°, FRP contribution is at the lowest level for all predictions. As the inclination of the FRP fibres decreases, the FRP contribution to ultimate strength starts to increase. The design guidelines and the model reach the maximum FRP contribution when inclination angle reaches to 45°. After exceeding inclination angle of 45°, contribution starts to decrease.

Inclination angle is influencing the CIDAR guideline in a different manner. The model uses cotangent values of inclination angle at the final formula. By way of that, the effect of inclination angle reasons a different behavior over ultimate shear behavior.

4.5. Influence of the FRP thickness

The thickness of FRP is another factor that affects directly the strength and stiffness of the strengthening material. Therefore FRP thickness has a significant influence on the FRP contribution. FRP thickness can be defined as a layer or layers of fiber bonded in a matrix of epoxy resin. The variations of the predicted FRP contribution versus FRP thickness for design guidelines are shown in Fig. 8. As expected, FRP contribution increases with the increase of thickness of FRP reinforcements. Besides, there is a similarity between ACI 440.2R, CIDAR and fib14 predictions since the curves follow a similar tendency.

4.6. Influence of the shear span-to-depth ratio

The influence of shear span-to-depth ratio (a/d) was not considered by some design codes up to then. However, performed studies showed that a/d ratio is influencing the ultimate behavior directly [56–59]. The a/d ratio is so important that it could direct the ultimate behavior from deep beam to slender beam. Therefore, to designate the influence of a/d ratio, seven externally strengthened

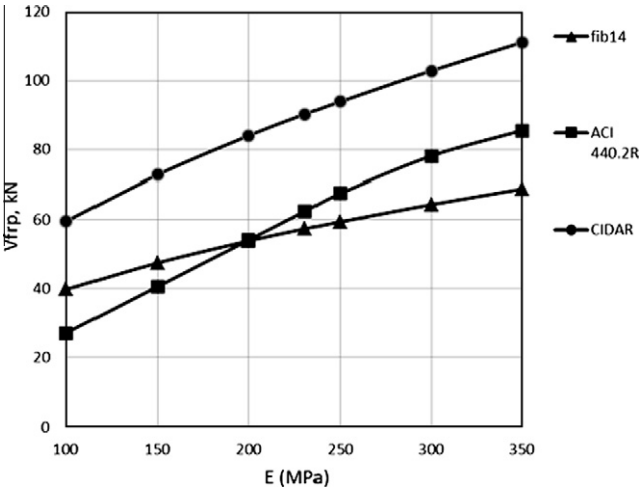

Fig. 6. Influence of the elastic modulus of the FRP reinforcement.

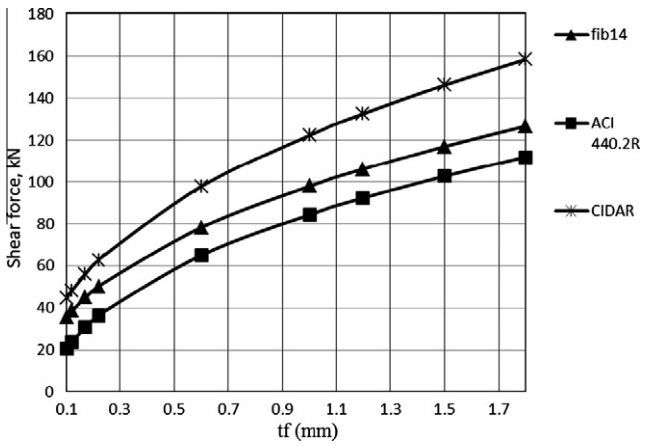

Fig. 8. Influence of the FRP thickness.

Fig. 9. Test for designating the influence of a/d.

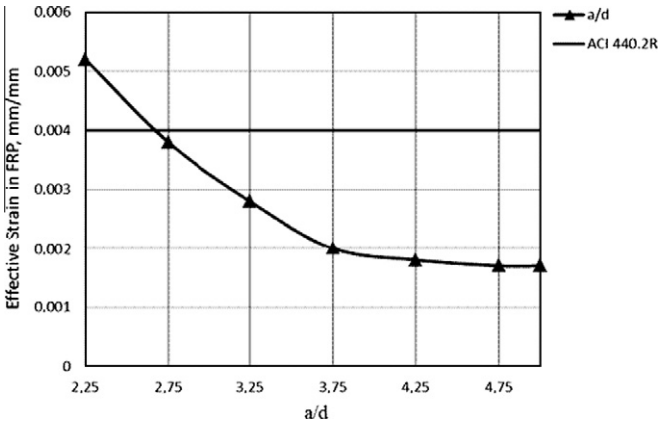

Fig. 10. Influence of the shear span-to-depth ratio.

specimens with different a/d ratios were tested under four point bending in the laboratory (Fig. 9). As the effect of a/d ratio for the shear strengthened beam is investigated, CFRP strengthened specimens were tested. The same unidirectional CFRP wraps and adhesive that were used for experimental tests were selected as strengthening materials for this test procedure. Rectangular beams consist of three 14 mm diameter bars in the compression zone and two 12 mm diameter bars in the tension zone. The shear span is 300 mm for all specimens. In order to obtain different a/d ratio, shear span is held constant and the effective height of test specimens are selected as variables. The tests results are plotted in Fig. 10. Strain values measured from beams with different a/d ratio showed that a/d ratio has a great influence on shear strength. Accordingly, as the ratio a/d increases, CFRP contribution to the shear strength of strengthened beams decreases. Therefore, in order to obtain conservative results with the ANN model predictions and the test results, the effect of a/d ratio was considered while building up the ANN model.

5. Neural network models of FRP strengthened beams

The selection of optimal configuration of ANN is the key point to achieve successful results from the suggested ANN model. Therefore, the mechanical properties of strengthening material and mechanical and dimensional properties of experimental beams are selected as inputs. In the literature, the strengthened specimens' concrete strength is generally above 20 MPa. In addition, some guidelines [30] do not propose to use FRP strengthening technique (due to the bond problems) to the structures with compressive strength below 17 MPa. However, the concrete strength of buildings that require retrofitting is generally lower than the pre mentioned value. In this study, the structures that have low concrete compressive strength are also accounted in the proposed ANN model in order to achieve the aspects of strengthening philosophy. Therefore, experimental data that will direct ANN model to evaluate such structures was especially collected from literature.

The aim of strengthening is to advance the behavior and increase the strength of deficient specimens. However, if the strengthening scheme is not selected properly, the specimen can fail in shear under increasing loads although the strengthening scheme is U-jacketing. Data of U-jacketed specimens that were failed due to shear are also added to the ANN model. Thus, ANN model estimates the shear capacity of specimens in a manner that if the specimen will reach or not reach its flexural capacity.

The neural network model is built by considering these approaches and it contains nine input nodes, representing the parameters of the width of the beam (b_w; mm), the effective height of the beam (d; mm), concrete compressive strength of specimen (f'_c; MPa), type of wrapping scheme (w_f/s_f), the angle between the principal fiber orientation and the longitudinal axis of the member (β), the elastic modulus of the FRP reinforcement (E_f; MPa), design rupture strain of FRP reinforcement (ε_{fu}; mm/mm), and total fabric design thickness (t_f; mm) and shear span-to-depth ratio (a/d).

The model have one hidden layer with four nodes, and output layer with one node giving contribution of FRP reinforcements. The structure of Neural Network model is presented in Fig. 11. Since the sigmoid function is used as transfer function, the inputs as well as the output are scaled in the range of 0–1.0. The training of networks is performed by using 51 sets of data selected from 84 data that is collected from the literature. The remaining randomly selected 33 data sets are used for testing of the networks. The database used for both training and testing patterns is presented in

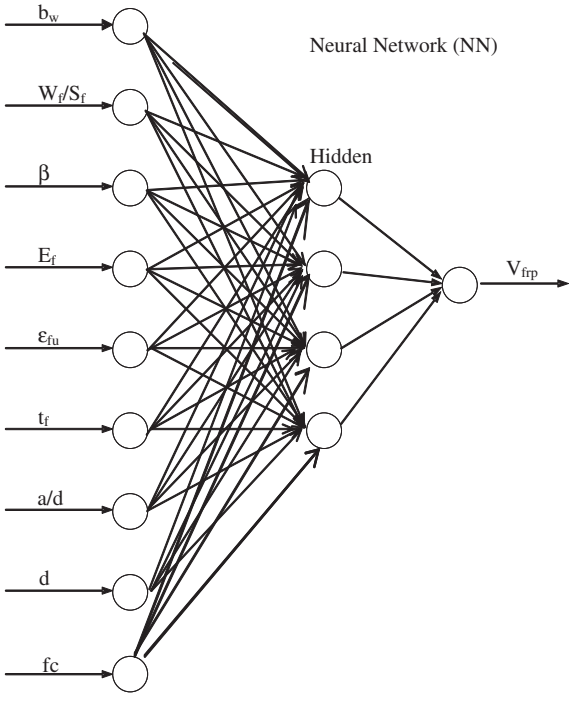

Fig. 11. The structure of NN.

Table 2
The summarization of theoretical guideline equations.

Design guide	General expression	U	w	Comments
ACI 440.2R	$V_f = \phi \cdot \varphi_f \left(2 \cdot t_f \cdot \frac{w_f}{s_f} \cdot f_{fe} \cdot (\sin\beta + \cos\beta) \cdot d_f\right)$ $\phi = 0.85, \varphi_f = 0.85$	$\varepsilon f_e = k_v \cdot \varepsilon_{fu} \leqslant 0.004$	$\varepsilon_{fe} = 0.004 \leqslant 0.75 \cdot \varepsilon_{fe}$	$k_v = \frac{k_1 \cdot k_2 \cdot L_e}{11900 \cdot \varepsilon_{fu}} \leqslant 0.75, L_e = \left(\frac{23300}{(t_f \cdot E_f)^{0.58}}\right)$ $k_1 = \left(\frac{f_{ck}}{27}\right)^{2/3} \quad k_2 = \frac{d_f - L_e}{d_f}$
CNR-DT200	$V_f = \frac{1}{\gamma_{Rd}} \cdot 0.9 \cdot d \cdot f_{fed} \cdot 2 \cdot t_f \cdot (\cot\theta + \cot\beta) \frac{w_f}{s_f}$	$f_{fed} = f_{fdd} \cdot 1 - \frac{1}{3} \cdot \frac{L_e \sin\beta}{\min\{0.9 \cdot d; h_w\}}$	$f_{fed} = f_{fdd} \cdot 1 - \frac{1}{6} \cdot \frac{L_e \sin\beta}{\min\{0.9 \cdot d; h_w\}} + \frac{1}{2} \cdot (\phi_R \cdot f_{fu} - f_{fdd}) \cdot \left(1 - \frac{L_e \sin\beta}{\min\{0.9 \cdot d; h_w\}}\right)$	$L_e = \sqrt{\frac{E_f \cdot t_f}{2 \cdot f_{ctm}}}, \phi_R = 0.2 + 1.6 \frac{r_c}{b_w}, 0 \leq \frac{r_c}{b_w} \leq 0.5$ $f_{fdd} = \frac{0.80}{\gamma_{fd}} \sqrt{\frac{2 \cdot E \cdot G_{fk}}{t_f}}, Gfk = 0.03 \cdot k_b \sqrt{f_{ck} \cdot f_{ctm}}, \quad kb = \frac{\sqrt{2 - wf/sf}}{1 + bf/400}$
fib14	$V_f = 0.9 \cdot \varepsilon_{fed} \cdot E_f \cdot \rho_t \cdot b_w \cdot d \cdot (\cot\theta + \cot\beta), \sin\beta$	$\varepsilon_{fe} = \min \begin{pmatrix} 0.65 \cdot \left(\frac{(cm^{2/3})}{E_f \cdot \rho t}\right)^{0.56} \cdot 10^{-3} \\ 0.17 \cdot \left(\frac{(cm^{2/3})}{E_f \cdot \rho t}\right)^{0.30} \cdot \varepsilon_{fu} \end{pmatrix}$	$\varepsilon_{fe} = 0.17 \cdot \left(\frac{(cm^{2/3})}{E_f \cdot \rho t}\right)^{0.30} \cdot \varepsilon_{fu}$	$\rho t = \frac{2 \cdot f \cdot w_f}{b_w \cdot s_f}, \varepsilon_{fed} = \frac{0.8 \varepsilon_{fe}}{\gamma_f}$
	$V_f = 2 \cdot f_{fed} \cdot t_f \cdot \frac{w_f}{s_f} \cdot h_{fe} \cdot (\cot\theta + \cot\beta) \cdot \sin\beta$	$D_f = \begin{pmatrix} \frac{2}{\pi \cdot \lambda} \cdot \frac{1 - \cos(\frac{\pi}{2} \cdot \lambda)}{\sin(\frac{\pi}{2} \cdot \lambda)}, \lambda \leqslant 1 \\ 1 - \frac{2}{\pi \cdot \lambda}, \lambda \geqslant 1 \end{pmatrix} \quad \lambda = l_{max}/L_e$ $l_{max} = h_{fe}/\sin\beta$ $l_e \sqrt{(E_f \cdot t_f)/\sqrt{f'ck}}$	$D_f = 0.5\left(1 + \frac{z_t}{h}\right)$	
CIDAR	$h_{fe} = z_b - z_t, z_b = 0.9 \cdot d - d_{fp}, z_t = d_{ft}$		$f_{fd,max} = \begin{pmatrix} \frac{1}{\gamma_f} \cdot \phi_R \cdot f_{fu} \cdot \varepsilon_f \leq 1.5\% \\ \frac{1}{\gamma_f} \cdot \phi_R \cdot E_f \cdot f_{fu} \cdot \varepsilon_f \leq 1.5\% \end{pmatrix}$	$f_{fed} = D_f \cdot f_{fd,max}$
	$V_f = \phi_{frp} \cdot \varepsilon_{frp} \cdot E_{frp} \cdot A_{frp} \cdot d_{frp} \cdot \frac{(\sin\beta + \cos\beta)}{sfrp}$	$R = \alpha\lambda_1 \left(\frac{f_c^{2/3}}{\rho_{frp} \cdot E_{frp}}\right) \varepsilon_{frpu_r} = \frac{\alpha \cdot k_1 \cdot k_2 \cdot L_e}{9525},$	$\phi_R = 0.80; \gamma_f = 1.25$	$\varepsilon_{fe} = R \cdot \varepsilon_{frpu} \leqslant 0.004$
CHBDC	$\lambda_1 = 1.35, \lambda_2 = 0.30$ for CFRP,	$L_e = \left(\frac{23350}{(t_f \cdot E_f)^{0.58}}\right)$	$R = \alpha\lambda_1 \left(\frac{f_c^{2/3}}{\rho_{frp} \cdot E_{frp}}\right), L_e = \left(\frac{23350}{(t_f \cdot E_f)^{0.58}}\right) \cdot k_1 = \left(\frac{f_{ck}}{27.65}\right)^{2/3} k_2 = \frac{dfrp - L_e}{d_f}$	
	$\lambda_1 = 1.23, \lambda_2 = 0.47$ for CFRP	$k_1 = \left(\frac{f_{ck}}{27.65}\right)^{2/3} \quad k_2 = \frac{dfrp - L_e}{d_f}$		

Tables A1 and A2 in Appendix A. The convergence of the models in training is based on minimizing the error of tolerance for root mean squared error (RMSE) during the training cycles and monitoring the overall the performance of the trained networks by comparing the outputs.

6. Analytical formulations for FRP shear reinforcement design

The use of FRP composites for strengthening is an advance and innovative strengthening technique. As a result of increasing demand and popularity, various analytical equations are developed in order to achieve adequate designs for installation and detailing of FRP based strengthening systems. Even though, the behavior of stirrups and FRP reinforcements show different behaviors basically, guidelines generally addressed the truss analogy for predicting the FRP contribution to the shear strength. All stirrups intersected by the critical shear crack may reach their yield strength at the same time and the stress distribution in steel stirrups along the intersecting critical shear crack is uniform. On the other hand, the bond length of the FRP's, which affects the stress in FRP directly, is irregular depending on the crack angle for the FRP strengthened members. Besides, FRP strengthened concrete member is not able to perform further plastic deformation due to the brittle behavior of FRP and concrete. Thus, the stress distribution in the FRP along the shear crack is not uniform and the maximum stress is limited by the ultimate tensile strength of FRP.

From the investigations based on the failed specimens, the maximum stress of the FRP is significantly smaller than the ultimate tensile strength of FRP at the ultimate state [60,61]. Therefore, effective stress in the FRP intersected by the critical shear crack at the ultimate state is the key parameter for predicting the exact contribution of FRP. The main difference between the guidelines is mainly about the technique that is used to predict the effective stress at ultimate state. In prediction of effective stress, guidelines consider many parameters as affecting the bond behavior of laminates. The elasticity and rigidity of the FRP laminate are the main parameters that affect the bond behavior of laminates.

Shear cracks can be controlled by limiting the strain level. From this perspective, the shear resistance of a beam can be calculated by adding the shear resistances of the concrete and shear reinforcement independently. Besides, guidelines make a further assumption and added the contribution of FRP directly to the shear resistance of a beam. As a result, the shear strength of a strengthened RC section is expressed as the sum of the three shear components in international guidelines and given in Eq. (5).

$$V_n = V_c + V_s + V_f \tag{5}$$

where V_c is the contribution of concrete, V_s is the contribution of internal steel shear reinforcement and finally V_f is the contribution of FRP to shear strength of RC section. The calculation procedure of V_f is different for each design provisions. In this study, some of the well-known equations; International Federation for Structural Concrete (fib14) [38], the American guideline (ACI 440.2R) [39], the Australian guideline (CIDAR) [40], the Italian National Research Council (CNR-DT 200) [41] and Canadian guideline (CHBDC) [42] are selected for evaluation of ANN model. The summarization of theoretical guideline equations are presented in Table 2. The geometrical and configuration properties required to determine the shear capacity by the theoretical guideline equations are described in Fig. 12.

7. Predicted results using ANN and design proposals

In the present study, ANN network was trained using 51 data sets, they were then tested using 33 test data sets for verification

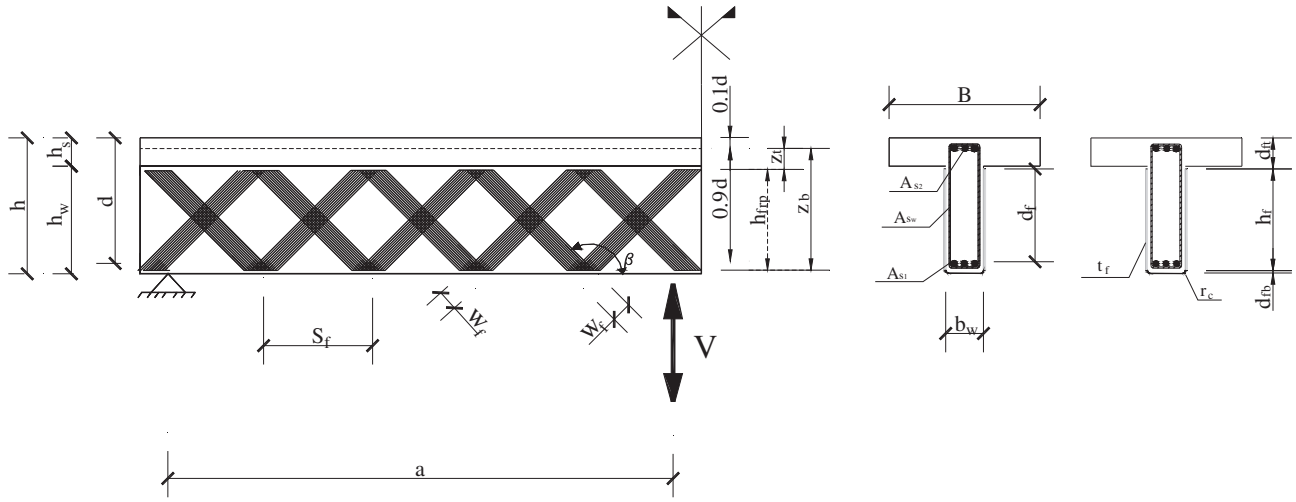

Fig. 12. Parametric notations of guideline equations.

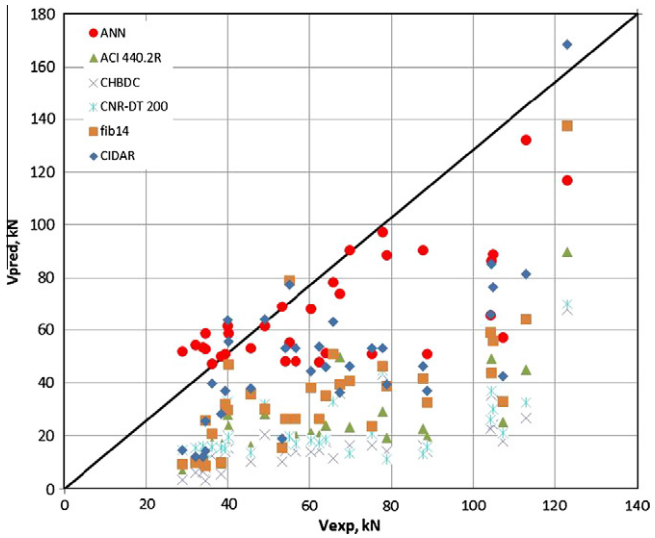

Fig. 13. Comparison of ANN predictions with theoretical guideline predictions.

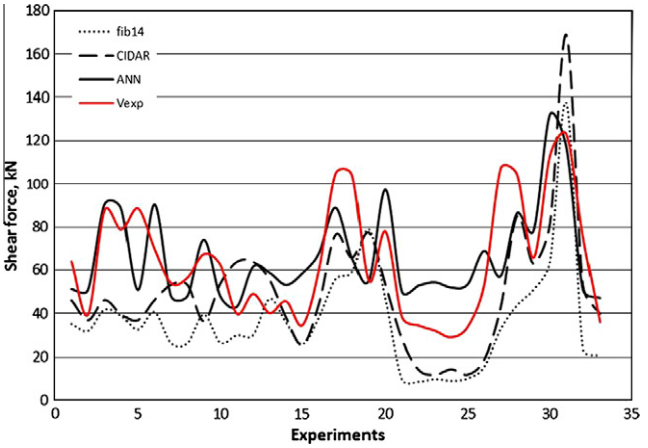

Fig. 14. Comparison of experimental results with ANN, fib14 and CIDAR predictions.

of results. The predicted ANN results are primarily compared with experimental FRP contribution of strengthened beams and then with those 'theoretical' predictions calculated directly from the FRP guidelines. Fig. 13 shows the predicted values versus experimental values of FRP contribution of beams from ANNs as well as those obtained from the fib14, ACI 440.2R, CIDAR, CNR-DT 200 and CHBDC building design guidelines. Accordingly, neural network model successfully build up a relation between the input parameters and the output (contribution of FRP) and predicted better than those obtained from the equations of the design guidelines.

Predictions of ACI 440.2R, CNR-DT 200 and CHBDC tend to underestimate the experimental shear strength in all of the cases of test data. Their predictions were not also close to the experimental results. CIDAR and fib14 provided more adequate results for predicting the FRP contribution according to the experimental results. 26% of theoretically calculated fib14 results fall within ±25% of the experimental shear strength. However, the results are mainly under the unity line, indicating that guideline predominantly underestimate the FRP contribution. Best predictions were observed from CIDAR within the 'theoretical' predictions of FRP guidelines. CIDAR predictions showed somewhat similar trend with ANN predictions on the other hand they are less scattered. Accordingly, 5% of CIDAR predictions are within 5% of the experimental results and also, 29% of the CIDAR predictions are within ±25% of the measured values.

ANN model was predicted the FRP contribution without too much deviation. Its predictions were close to the experimental FRP contributions and plotted on either side of the desired ratio of 1 (Fig. 13). In addition, 7.5% of ANN predictions are within 5% of the experimental results and also, 49% of the ANN predictions are within ±25% of the measured values. It is clear that the neural network model is capable of predicting the experimental FRP contribution better than the other considered methods for all the data range covered in the training sets. A large number of experimental data is used to train the ANN and the obtained results are adequately fitting to the experimental results. Therefore, it is proposed to use ANN model for predicting the FRP contribution for the wrapped and U-jacketed deficient RC beams.

Statistical analyses are also carried out for evaluating the efficiency of ANN and analytically calculated results via comparison to experimental results. fib14 and CIDAR are selected for statistical analyses as their predictions were seemed more adequate to the experimental results than the other considered design guidelines. While evaluating the convenience of predicted results with the

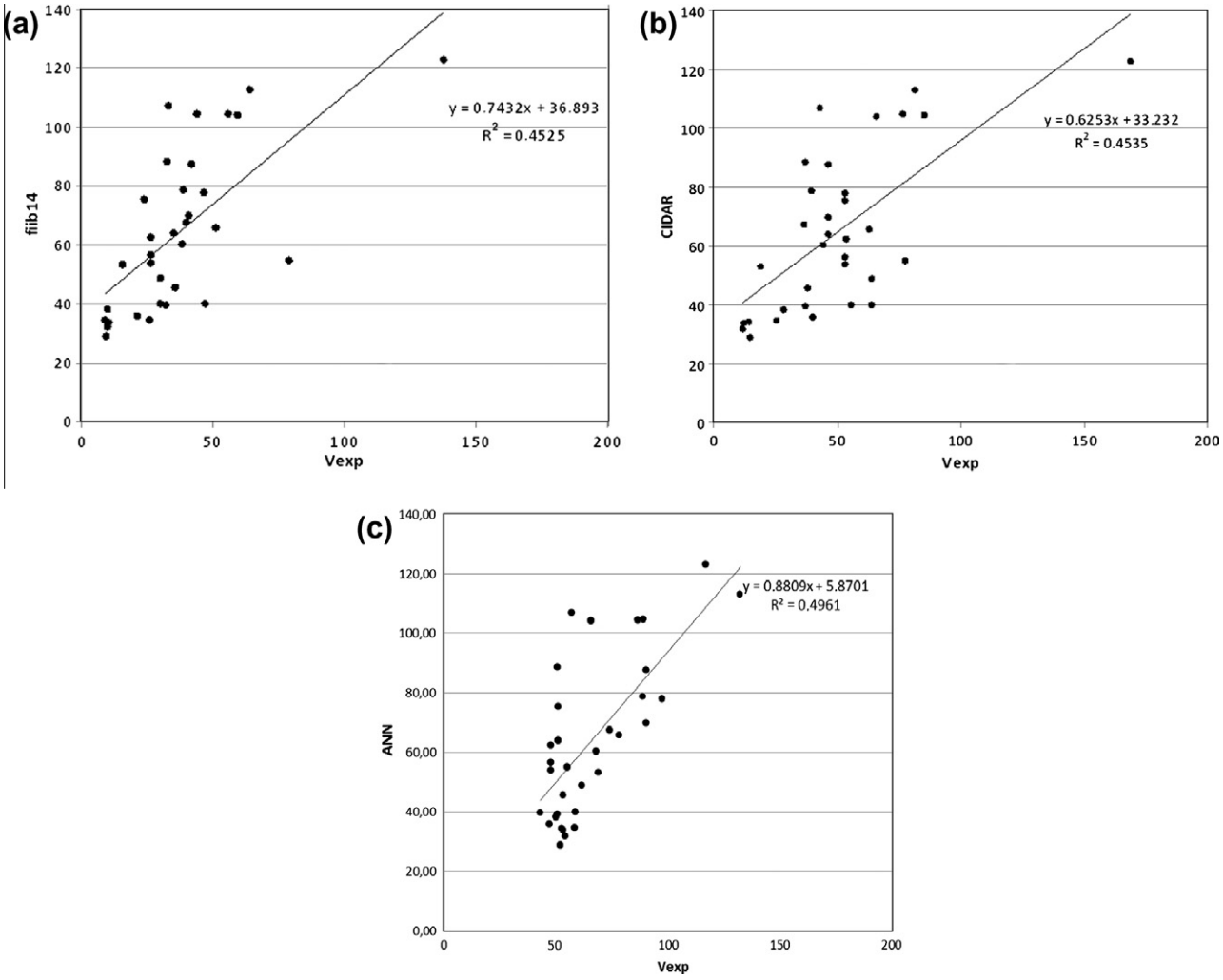

Fig. 15. Behavior of ANN, fib14 and CIDAR results.

experimental results, three factors are considered. These are consistency in means, consistency in standard deviations and distribution of residuals. It must be point out that the distribution of the residuals will be homogeneous if the mean and extreme values are well represented in the evaluated data. Extreme values of analytically calculated results will also help to ensure the reliability of results and their compliance with the estimated calculation methods.

The theoretical and calculated results of fib14, CIDAR and ANN are plotted in Fig. 14 with the comparison of experimental results. As it can be seen from the plots, theoretical results of fib14 and CIDAR are close to the experimental results but almost at every step they underestimated the experimental results. However, ANN predictions are around the experimental values and so regularity of the proposed ANN method is higher according to the design guideline predictions.

The root mean square error (RMSE) is a quadratic scoring rule which measures the average magnitude of the error. It gives a relatively high weight to large errors. This means the RMSE is most useful when large errors are particularly undesirable. In addition, RMSE values are also useful to determine how close theoretical results get to the experimental results.

$$\mathrm{RMSE} = \sqrt{\sum_{i=1}^{n} e_i^2/n} \tag{6}$$

$$e_i = V_{f,\mathrm{calculated}} - V_{f,\mathrm{experimental}} \quad i = 1,\ldots,n \tag{7}$$

where e_i indicates the difference between calculated and experimental results and n is the number of data that is used for calculation. In order to evaluate the trustworthiness of the predicted results, the interactive results of fib14, CIDAR and ANN with experimental results are examined with the experimental results. Accordingly, RMSE results of ANN, CIDAR and fib14 are 19.55, 26.74 and 34.30, respectively. As it can be realized; ANN produced the lowest RMSE results when compared to the calculated theoretical results. This situated the success of ANN model as it produces closer predictions on average than that of the theoretical guidelines.

$$\mathrm{RMSE}_{\mathrm{ANN}} < \mathrm{RMSE}_{\mathrm{CIDAR}} < \mathrm{RMSE}_{\mathrm{FIB14}} \tag{8}$$

Coefficient of determination shows the linear relationship between two series. Although the ultimate shear behavior of FRP strengthened RC structures is not linear, the linear or nonlinear relationship between theoretical guidelines and experimental results as well ANN results are investigated. The linear relationship between theoretical results and experimental results is defined by the help of coefficient of determination in Eq. (9).

$$D = R^2 = \frac{\sum_{i=1}^{n}(\widehat{V}_{f,i} - \overline{V}_f)^2}{\sum_{i=1}^{n}(V_{f,i} - \overline{V}_f)^2} \tag{9}$$

Table A1
Geometrical and material properties of the experimental RC beams.

Ref.	Spec.	Geometric data			Type	FRP thickness	Young modulus	Tensile strength	Strength scheme[a]	$\frac{w_{frp}^2}{S_{frp}Sin\beta}$ [b]	V_f (kN)
		b (mm)	h (mm)	d (mm)	R–T	t_{frp} (mm)	E_{frp} (GPa)	f_{ftp} (MPa)			
	(1)	(2)	(3)	(4)	(5)	(6)	(7)	(8)	(9)	(10)	(11)
[14]	SB3-90	230	380	343	R	0.18	228	4104	W-P90	1.00	65.01
	SB5-90	230	380	343	R	0.18	228	4104	W-P90	1.00	70.92
	SB6-90	230	380	343	R	0.18	228	4104	W-P90	1.00	38.42
	SB9-90	230	380	343	R	0.18	228	4104	W-P45	1.41	130.02
	SB10-45	230	380	343	R	0.18	228	4104	W-P45	1.41	147.75
	SB11-45	230	380	343	R	0.18	228	4104	W-P45	1.41	110.32
	SB12-45	230	380	343	R	0.18	228	4104	W-P45	1.41	131.99
[15]	BT2	150	405	371	T	0.165	228	3876	U-P90	1.00	65.00
	BT3	150	405	370	T	0.165	228	3876	U-P90	1.00	67.50
	BT4	150	405	371	T	0.165	228	3876	U-S90	0.40	72.00
	BT6	150	405	371	T	0.165	228	3876	W-P90	1.00	131.00
[16]	AS1	150	300	272	R	0.044	73	2628	W-P90	1.00	27.50
	AS2	150	300	272	R	0.044	73	2628	W-S90	0.50	26.00
	AS3	150	300	272	R	0.088	73	2628	W-P90	1.00	49.40
	CS1	300	300	257	R	0.111	244	4148	W-P90	1.00	109.80
	CS2	300	300	257	R	0.111	244	4148	W-S90	0.50	54.80
	CS3	150	300	257	R	0.111	244	4148	W-S90	0.50	51.40
	AB1	150	300	253	R	0.044	73	2628	W-P90	1.00	62.00
	AB2	300	300	253	R	0.044	73	2628	W-P90	1.00	38.00
	AB4	300	300	253	R	0.088	73	2628	W-P90	1.00	92.80
	AB5	300	300	253	R	0.144	73	2628	W-P90	1.00	122.00
	AB6	300	300	253	R	0.22	73	2628	W-P90	1.00	115.00
	AB7	300	300	253	R	0.264	73	2628	W-P90	1.00	108.00
	AB8	600	300	253	R	0.144	73	2628	W-P90	1.00	130.20
	AB9	450	450	399	R	0.144	73	2628	W-P90	1.00	161.50
[17]	BS2	200	450	395	R	0.11	240	3360	U-S90	0.25	41.10
	BS5	200	450	395	R	0.11	240	3360	U-S90	0.13	33.80
	BS6	200	450	395	R	0.11	240	3360	U-S90	0.08	31.20
	BS7	200	450	395	R	0.11	240	3360	W-S90	0.25	100.70
[18]	A10-M	150	300	285	R	0.334	390	3120	U-S90	0.13	21.34
	A12-M	150	300	285	R	0.334	390	3120	U-S90	0.26	61.96
	B10-M	150	150	135	R	0.334	390	3120	U-S90	0.31	36.56
	B12-M	150	150	135	R	0.334	390	3120	U-S90	0.63	66.29
[19]	USV+	250	450	420	R	0.22	390	3120	U-S45	0.53	36.45
	US45+	250	450	420	R	0.22	390	3120	U-S45	0.50	27.58
	LTF90	250	450	420	R	0.22	390	3120	U-S90	0.50	26.60
	US45++	250	450	420	R	0.22	390	3120	U-S45	0.47	35.46
	WS45++	250	450	420	R	0.22	390	3120	W-S45	0.47	60.09
	US45+"A"	250	450	420	R	0.22	390	3120	U-S45	0.94	67.97
	US45++"B	250	450	420	R	0.22	390	3120	U-S45	0.94	72.89
	US45++"C	250	450	420	R	0.22	390	3120	U-S45	0.94	83.73
	US45++"E"	250	450	420	R	0.22	390	3120	U-S45	0.71	64.03
[20]	CO2	150	305	264	R	0.165	228	3876	U-S90	0.40	40.00
	CO3	150	305	264	R	0.165	228	3876	U-P90	1.00	65.00

[a] U: U-Jacketed. W: Wrapped. S: Strips. P:Plate. #: orientation angle of fibres.
[b] W_{frp}: width of strips. S_{frp}: spacing.
$*$ Test data sets.

Table A2
Geometrical and material properties of the experimental RC beams.

Ref.	Spec.	Geometric data			Type	FRP thickness	Young modulus	Tensile strength	Strength scheme[a]	$\frac{w_{frp}^2}{S_{frp}Sin\beta}$ [b]	V_f (kN)
		b (mm)	h (mm)	d (mm)	R–T	t_{frp} (mm)	E_{frp} (GPa)	f_{frp} (MPa)			
	(1)	(2)	(3)	(4)	(5)	(6)	(7)	(8)	(9)	(10)	(11)
[21]	B-CF2	150	305	265	R	0.165	228	3876	U-P90	1.00	26.00
	B-CF4	150	305	266	R	0.165	228	3876	W-P90	1.00	47.00
	A-SO3-2*	150	305	264	R	0.165	228	3876	U-S90	0.40	54.00
	A-SO3-3*	150	305	264	R	0.165	228	3876	U-S90	0.40	56.50
	A-SO3-4*	150	305	265	R	0.165	228	3876	U-P90	1.00	67.50
	A-SO4-2*	150	305	266	R	0.165	228	3876	U-S90	0.40	62.50
[22]	PU1*	130	450	425	R	0.43	105	1365	U-S90	0.20	64.03
	PU2*	130	450	425	R	0.43	105	1365	U-S90	0.16	39.40
	PU3*	130	450	425	R	0.43	105	1365	U-S45	0.19	87.67
	PU4*	130	450	425	R	0.43	105	1365	U-S45	0.16	78.80
	PC2*	130	450	425	R	0.43	105	1365	W-S90	0.16	88.65
	PC3*	130	450	425	R	0.43	105	1365	W-S45	0.19	69.94
[23]	BEAM-2*	120	360	335	T	0.12	231	3927	U-S90	0.63	39.87
	BEAM-5*	120	360	335	T	0.12	231	3927	U-P90	1.00	49.03
[24]	BEAM-8*	200	350	320	R	0.12	231	3927	W-S90	0.42	40.10
[25]	CF-045*	200	400	320	R	0.111	230	3450	W-S90	0.23	34.60
	CF-064*	200	400	320	R	0.111	230	3450	W-S90	0.41	60.40
	CF-097*	200	400	320	R	0.111	230	3450	W-S90	0.70	104.7
[26]	No. 2*	250	500	400	R	0.111	244	3904	W-S90	0.40	104.2
	No. 3*	250	500	400	R	0.169	90	2880	W-S90	0.40	55.00
	No. 2*	250	600	560	R	0.033	246	2706	W-P90	1.00	77.90
[27]	AI*	60	190	153	R	1.041	11	220	U-P90	1.00	38.36
	EI*	60	190	153	R	0.66	14.3	171.6	U-P90	1.00	34.46
	GI*	60	190	153	R	0.584	21	168	U-P90	1.00	32.01
	E2*	60	190	153	R	0.66	14.3	171.6	U-P90	1.00	28.98
	G2*	60	190	153	R	0.584	21	168	U-P90	1.00	33.84
	45G2*	60	190	153	R	0.584	21	168	U-P45	1.41	53.21
[28]	S3*	200	300	260	R	0.11	230	3450	U-S90	0.50	107.1
	S5*	200	300	260	R	0.11	230	3450	U-P90	1.00	104.4
[29]	No. 3*	150	400	232	T	0.111	230	3450	U-P90	1.00	65.80
[30]	SB3*	300	300	260	R	0.11	248	3472	W-P90	1.00	113.0
	SC2*	600	600	554	R	0.11	230	2760	W-P90	1.00	123.0
[31]	BT1-1I*	120	340	310	R	0.09	230	3910	U-S90	0.53	75.35
	BT1-2I*	120	340	310	R	0.09	230	3910	U-S90	0.40	36.04

[a] U: U-Jacketed. W: Wrapped. S: Strips. P: Plate. #: orientation angle of fibres.
[b] W_{frp}: width of strips. S_{frp}: Spacing.
* Test data sets.

where $\widehat{V}_{f,i}$ is the theoretically calculated FRP contribution, $V_{f,i}$ is experimental FRP contribution and $\overline{V}_f$ is the mean of FRP contribution that is obtained from experiments. As it is plotted in Fig. 15a–c, the coefficient of determination parameter of ANN model is slightly greater than the compared proposals (Eq. (10)). This indicates that ANN model is more linear and slightly more accurate with respect to the design codes within the range of parameters covered in the study.

$$D_{\text{ANN}} > D_{\text{CIDAR}} > D_{\text{fib14}} \tag{10}$$

In addition to the above-mentioned criteria, basic statistical terms of theoretical and ANN results are investigated by considering the residuals. The average value helps to summarize the relevant features of experimental results and it is calculated as 64.42. The average value of ANN, CIDAR and fib14 are 66.47, 49.88 and 37.84, respectively. As it can be seen, the average value of ANN results is found to be very close to the experimental results. Average residual term helps to find the range of relationships between two series. It must be point out that it is expected that average residual term is to be zero from a well build method. Accordingly, the average calculated residual term for the ANN results is 2.05. However, CIDAR and fib14 codes are calculated 14.54 and 27.38 values for the average residual terms, respectively. Additionally, the standard deviation values that are calculated by the other two standard deviation calculation methods are smaller than the standard deviation of the residual terms. It shows that ANN produces sometimes higher and sometimes lower predictions than the experimental results but the results are always released around the mean.

$$\overline{V}_{\mu} \cong \overline{V}_{f,\text{ANN}} > \overline{V}_{f,\text{CIDAR}} > \overline{V}_{f,\text{FIB14}} \tag{11}$$

$$\bar{e}_{\text{ANN}} \cong 0 < \bar{e}_{\text{CIDAR}} < \bar{e}_{\text{FIB14}} \tag{12}$$

$$S_{e,\text{ANN}} < S_{e,\text{FIB14}} < S_{e,\text{CIDAR}} \tag{13}$$

All of statistical outcomes emphasizes that the obtained ANN results have good agreement with the experimental results. Therefore, it is proposed to use ANN model to determine the FRP contribution of strengthened RC beams with wrapped and U-jacketed FRP.

8. Conclusions

In this paper, the option of adopting artificial neural networks to predict the contribution of wrapped and U-jacketed FRP to shear strength of deficient RC beams is investigated. Although a/d ratio is one of the most efficient parameter that directly affects the ultimate shear behavior, guideline equations do not consider this important parameter. However, the ANN model accounts the effect of a/d ratio while its ultimate shear strength calculations. Besides, the main objective is to build an efficient and accurate ANN model with parameters which can easily be obtained. Accordingly, a neural network model with back-propagation is developed. The ANN predictions are compared with the experimental results and the results obtained from various guideline equations to assess the efficiency of the ANN models.

- The design guidelines consider safety factors and characteristic values while estimating the shear contribution of the strengthening materials. That is the main reason of calculating lower shear capacities according to experimental results. However, that does not query the reliability of code assumptions. By this means, structural engineers will always be on the safe side while retrofitting the deficient structures. Since, ANN model is produced by considering experimental results, it generates reliable results for different behaviors practically. For example, if the training network of ANN contains data of specimen with low concrete compression strength, specimen with different a/d ratios, etc. The ANN accounts that incomes and estimates close results for these situations. The ability to produce different solutions for different situations is the main advantage of ANN according to common code assumptions.
- A new ANN model was built in this study by considering the effect of a/d ratio and different concrete compressive strength over the ultimate FRP contribution. ANN results indicated that the new ANN model can produce close results according to experimental results. There exists also a similar study in which an ANN model was build up but with slightly less data [62]. This study was also produced close results with its experimental results. Accordingly, both studies indicate that ANN method is capable of predicting FRP contribution in a successful manner.
- Within all 'theoretical' predictions of design guidelines, CIDAR provided the best predictions compared to the experimental results. In addition, CIDAR predictions show somewhat similar trend with ANN predictions. On the other hand, they are also consistent.
- Some guidelines [39] do not propose to use FRP strengthening technique (due to the bond problems) to the structures with compressive strength below 17 MPa. However, the concrete strength of buildings that require retrofitting is generally lower than the pre mentioned value. Therefore, an ANN model is developed by considering the need of retrofitting structures with low concrete compressive strength in this study. Accordingly, obtained results showed that ANN model can successfully predict the FRP contribution for structures with low concrete compressive strength within acceptable limits.
- fib14 and CIDAR produced close predictions to the experimental results. However, at almost every step they underestimated the experimental results and this shows that their predictions are always on the safe side because of the safety factors that were used while calculation.
- Neural network model successfully build up a relation between the input parameters and the output and predicted better than those from the equations of the design guidelines. As a result, neural network models can comfortably be used to predict the FRP contribution within the range of parameters covered in this study.
- All of statistical outcomes emphasizes that the obtained ANN results have good agreement with the experimental results.

The application of ANNs to predict the capacity of shear deficient RC beams strengthened with wrapped and U-jacketed FRPs is still in its basic stage. However, this study has presented satisfying predictions compared with the guideline equations. Besides, the ANN model can easily be improved by adding new experimental data to the model.

Appendix A

See Tables A1 and A2.

References

[1] Barros JAO, Fortes AS. Flexural strengthening of concrete beams with CFRP laminates bonded into slits. Cem Concr Compos 2005;27(4):471–80.
[2] Chajes MJ, Theodore Jr A, Thomson, Januszka TF, Finch WW. Flexural strengthening of concrete beams using externally bonded composite materials. Constr Build Mater 1994;8(3):191–201.
[3] El-Hacha R, Silva Filho JN, Melo GS, Rizkalla SH. Effectiveness of near-surface mounted FRP reinforcement for flexural strengthening of reinforced concrete beams. Proceedings of the 4th international conference on advanced composite materials in bridges and structures (ACMBS IV), Calgary, Alberta, Canada (CD-ROM); July 20-23, 2004. 8p.
[4] Chaallal O, Nollet M-J, Perraton D. Shear strengthening of RC beams by externally bonded side CFRP strips. J Compos Constr 1998;2(2):111–3.

[5] Taerwe L, Khalil H, Matthys S. Behaviour of RC beams strengthened in shear by external CFRP sheets. Proceedings of the third international symposium non-metallic (FRP) reinforcement for concrete structures, vol. 1, Japan; 1997. p. 483–90.
[6] Swamy RN, Mukhopadhyaya P, Lynsdale CJ. Strengthening for shear of RC beams by external plate bonding. Struct Eng 1999;77(12):19–30.
[7] Triantafillou TC. Shear strengthening of reinforced concrete beams using epoxy-bonded FRP composites. ACI Struct J 1998;95(2):107–15.
[8] Mitsui Y, Murakami K, Takeda K, Sakai H. A study on shear reinforcement of reinforced concrete beams externally bonded with carbon fibre sheets. Compos Interfaces 1998;5(4):285–95.
[9] Uji K. Improving shear capacity of existing reinforced concrete members by applying carbon fibre sheets. Trans Jpn Concr Inst 1992;14:253–66.
[10] Smith ST, Teng JG. Shear-bending interaction in debonding failures of FRP-plated RC beams. Adv Struct Eng 2003;6(1):183–99. 17.
[11] Kotynia R. Debonding failures of RC beams strengthened with externally bonded strips. Proceedings of the international symposium on bond behaviour of FRP in structures; 2005. p. 247–55.
[12] Khalifa A, Alkhrdaji T, Nanni A, Lansburg A. Anchorage of surface mounted FRP reinforcement. Concr Int, ACI 1999;21(10):49–54.
[13] El-Mihilmy Mahmoud T, Tedesco Joseph W. Prediction of anchorage failure for reinforced concrete beams strengthened with fiber-reinforced polymer plates. ACI Struct J 2001;98(3):301–14.
[14] Alagusundaramoorthy P, Harik IE, Choo CC. Shear strengthening of R/C beams wrapped with CFRP fabric. Research report KTC-02-14/SPR 200-99-2F, University of Kentucky, Kentucky Transportation Center; August 2002.
[15] Khalifa A, Nanni A. Improving shear capacity of existing RC T section beams using CFRP composites. Cem Concr Compos 2000;22:165–74.
[16] Umezu K, Fujita M, Nakai H, Tamaki K. Shear behavior of RC beams with aramid fiber sheet. Proceedings of the III international symposium non metallic (FRP) reinforcement for concrete structures, Japan; 1997. p. 491–8.
[17] Taerwe L, Khalil H, Matthys S. Behavior of RC beams strengthened in shear by external CFRP sheets. In: Proceedings of the III international symposium non metallic (FRP) reinforcement for concrete structures. Japan; 1997. p. 483–90.
[18] Barros JAO, Dias SJE, Lima JLT. Efficacy of CFRP-based techniques for the flexural and shear strengthening of concrete beams. Cem Concr Compos 2007;29:203–17.
[19] Monti G, Liotta MA. Test and design equations for FRP-strengthening in shear. Constr Build Mater 2007;21:799–809.
[20] Khalifa A, Tumialan G, Nanni A, Belarbi A. Shear strengthening of continuous RC beams using externally bonded CFRP sheets. Proceedings of the 4th international symposium on FRP for reinforcement of concrete structures. Baltimore, USA; 1999. p. 995–1008.
[21] Khalifa A, Belarbi A, Nanni A. Shear performance of RC members strengthened with externally bonded FRP wraps. Proceedings (CD-ROM) of twelfth world conference on earthquake, Auckland, New Zealand; January 30–February 4, 2000. 8 pages.
[22] Diagana C, Li A, Gedalia B, Delmas Y. Shear strengthening effectiveness with CFF strips. Eng Struct 2003;25:507–16.
[23] Anil O. Strengthening of RC T-section beams with low strength concrete using CFRP composites subjected to cyclic load. Constr Build Mater 2008;22: 2355–68.
[24] Sakar G. Shear strengthening of RC beams subjected to cyclic load using CFRP strips. Composite Lett 2008;17(6):203–11.
[25] Araki N, Matsuzaki Y, Nakano K, Kataka T, Fukuyama H. Shear capacity of retrofitted RC members with continuous fibre sheets. Non-metallic (FRP) reinforcement for concrete structures, proceedings of the third international Symposium, vol. 1, Japan Concrete Institute, Sapporo, Japan; 1997. p. 512–22.
[26] Kamiharako A, Maruyama K, Takada K, Shimomura T. 'Evaluation of shear contribution of FRP sheets attached to concrete beams. Non-metallic (FRP) reinforcement for concrete structures. Proceedings of the third international symposium, vol. 1. Japan Concrete Institute, Sapporo, Japan; 1997. p. 491–8.
[27] Chajes MJ, Januszka TF, Mertz DR, Thomson TA, Finch WW. Shear strengthening of reinforced concrete beams using externally applied composite fabrics. ACI Struct J 1995;92(3):295–303.
[28] Sato Y, Ueda T, Kakuta Y, Tanaka T. Shear reinforcing effect of carbon fibre sheet attached to side of reinforced concrete beams. In: El-Badry MM, editor. Advanced composite materials in bridges and structures; 1996. p. 621–7.
[29] Sato Y, Ueda T, Kakuta Y, Ono S. Ultimate shear capacity of reinforced concrete beams with carbon fibre sheet. Non-metallic (FRP) reinforcement for concrete structures. Proceedings of the third symposium, Japan, vol. 1; 1997. p. 499–505.
[30] Sato Y, Ueda T, Kakuta Y, Ono S. Shear strengthening of existing reinforced concrete beams by CFRP sheet. Non-metallic (FRP) reinforcement for concrete structures. Proceedings of the third international symposium, vol. 1. Japan Concrete Institute, Sapporo, Japan; 1997. p. 507–513.
[31] Jayaprakash J, Abdul Samad Abdul Aziz, Abbasovich Ashrabov Anvar. Concrete shear beams with externally bonded bi-directional CFRP strips. Constr Buil Mater 2008;22:1148–65.
[32] Guang NH, Zong WJ. Prediction of compressive strength of concrete by neural networks. Cem Concr Res 2000;30:1245–50.
[33] Goh ATC. Prediction of ultimate shear strength of deep beams using neural networks. ACI Struct J 1995;92(1):28–32.
[34] Sanad A, Saka MP. Prediction of ultimate shear strength of reinforced concrete deep beams using neural networks. J Struct Eng, ASCE 2001;127(7):818–28.
[35] Jamal A, Abdalla A, Elsanosi A. Abdelwahab. Modeling and simulation of shear resistance of R/C beams using artificial neural network. J Franklin Inst 2007;344:741–56.
[36] Ghaboussi J, Garret Jr JH, Wu X. Knowledge-based modeling of material behavior with neural networks. J Eng Mech, ASCE 1991;117(1):132–53.
[37] Hajela P, Berke L. Neuro-biological computational models in structural analysis and design. Comp Struct 1991;41(4):657–67.
[38] Fib. Bulletin 14 – externally bonded FRP reinforcement for RC structures. Technical report. Task Group 9.3 FRP (fibre reinforced polymer) reinforcement for concrete structures; 2001.
[39] ACI Committee 440 Report. Guide for the design and strengthening of externally bonded FRP systems for strengthening concrete structures. American Concrete Institute Committee; October 2001.
[40] CIDAR – Design guideline for RC structures retrofitted with FRP and metal plates: beams and slabs. Draft 3 – submitted to Standards Australia, The University of Adelaide; 2006.
[41] CNR-DT200. Guidelines for design, execution and control of strengthening interventions by means of fibre reinforced composites. National Research Council; 2004.
[42] Canadian Standards Association. Design and construction of building components with fiber-reinforced polymer, CSA-S806-02, Rexdale, Ontario, Canada; 2002. p. 2002.
[43] Perera R, Vıque J, Arteaga A, Diego A. Shear capacity of reinforced concrete members strengthened in shear with FRP by using strut-and-tie models and genetic algorithms. Composites Part B 2009;40(8):714.
[44] ACI Committee 318. Building code requirements for structural concrete, American Concrete Institute Committee; 2005. p. 430.
[45] Chen JF, Teng JG. Shear capacity of FRP strengthened RC beams: FRP debonding. Constr Build Mater 2003;17(1):27–41.
[46] Lippman R. An introduction to computing with neural networks. IEEE ASSP Mag 1987;4:4–22.
[47] Chow T, W S. Neural networks and computing, series in electrical and computer engineering, vol. 7. ISBN:978-1-86094-758-2.
[48] Haykin S. Neural networks: a comprehensive foundation; July 16, 1998. ISBN-13:978-0132733502.
[49] Anderson JA. An introduction to neural networks; March 16, 1995. ISBN-13:978-0262011440.
[50] Rumelhart DE, Hinton GE, ve Williams RJ. Learning internal representations by error propagation. In: Rumelhart DE, McClelland JL, editors. Parallel distributed processing: explorations in the microstructure of cognition, vol. 1. Cambridge, MA: MIT Press; 1986. chapter 8.
[51] Hecht-Nielsen R. Theory of the backpropagation neural network. IJCNN international conference on neural networks, vol. 1; 1989. p. 593–606.
[52] Jung Insung, Wang Gi-Nam. Pattern classification of back-propagation algorithm using exclusive connecting network. World Academy of Science, Engineering and Technology, vol 36; 2007. p. 189–93.
[53] Patterson DW. Artificial neural networks, theory and applications. Singapore: Prentice Hall; 1996.
[54] Fausett L. Fundamentals of neural networks: architectures, algorithms, and applications. Upper Saddle River, New Jersey: Prentice-Hall; 1994. 462.
[55] Higham DJ, Higham NJ. MATLAB guide. Philadelphia: SIAM; 2000.
[56] Li A, Diagana C, Delmas Y. CFRP contribution to shear capacity of strengthened RC beams. Eng Struct 2001;23:1212–20.
[57] Chaallal O, Shahawy M, Hassan M. Performance of reinforced concrete T-girders strengthened in shear with carbon fiber-reinforced polymer fabric. ACI Struct J 2002(May–June):335–43.
[58] Khalifa A, Nanni A. Rehabilitation of rectangular simply supported RC beams with shear deficiencies using CFRP composites. Constr Build Mater 2002;16: 135–46.
[59] Jayaprakash J, Samad AAA, Abbasovich AAA, Ali AAA. Shear capacity of precracked and non precracked reinforced concrete shear beams with externally bonded bi-directional CFRP strips. Constr Build Mater 2007;22(6): 1148–65.
[60] Tanarslan H, Altin M, Ertutar S. The effects of CFRP strips for improving shear capacity of RC beams. J Reinf Plast Compos 2008;27(12):1287–308.
[61] Tanarslan HM. Behavior of RC beams strengthened with inclined CFRP strips. J Reinf Plast Compos 2010. doi:10.1177/0731684410371406.
[62] Perera R, Vıque J, Arteaga A, Diego. Artificial intelligence techniques for prediction of the capacity of RC beams strengthened in shear with external FRP reinforcement. Compos Struct 2010;92:1169–75.